Hindawi
Advances in Polymer Technology
Volume 2023, Article ID 9452164, 9 pages
https://doi.org/10.1155/2023/9452164

Research Article

Physicochemical Characteristics of Chitosan–Alginate Scaffold Containing Atorvastatin

Hananeh Hamedfar,[1] Tayebeh Zivari-Ghader,[1] Abolfazl Akbarzadeh,[2] and Soodabeh Davaran[1,3]

[1]*Department of Medicinal Chemistry, Faculty of Pharmacy, Tabriz University of Medical Sciences, Tabriz, Iran*
[2]*Faculty of Pharmacy, Department of Medicinal Chemistry and Drug Applied Research Center, Tabriz University of Medical Sciences, Tabriz 51368, Iran*
[3]*Department of Toxicology, Faculty of Pharmacy, Yeditepe University, Ataşehir, Istanbul, Turkey*

Correspondence should be addressed to Soodabeh Davaran; davaran@tbzmed.ac.ir

Hananeh Hamedfar and Tayebeh Zivari-Ghader contributed equally to this work.

Received 19 November 2022; Revised 25 April 2023; Accepted 7 August 2023; Published 30 August 2023

Academic Editor: Chang Chuan Lee

In addition to being a lipid-lowering medication, atorvastatin (ATV) is an anti-inflammatory agent. When there is a bone defect or inflammation of adjacent tissues, it aids in bone repair. This study aimed to develop a chitosan–alginate (CS/ALG)–tripolyphosphate (TPP)–ATV hybrid hydrogel as a drug delivery system, using a tissue engineering scaffold for the first time. For this purpose, a CS/ALG hydrogel crosslinked with TPP was developed. The delivery profile of ATV and its physicochemical properties such as particle size and hydrogel swelling percentage were determined. The structure and morphology of the hydrogels were analyzed using Fourier transform infrared spectroscopy and scanning electron microscopy. As a result, an alginate–chitosan hydrogel with a TPP crosslinker was prepared. The results revealed that drug loading was nearly complete, and the first hour revealed a 25% explosive release. The drug was gradually released over 10 hr at approximately 35%. The amount of crosslinker used significantly influenced the encapsulation gain and release profiles. Owing to its high porosity and swelling, the CS/ALG hydrogel crosslinked with PPT is an ideal scaffold for loading drugs, macromolecules, and cells.

1. Introduction

Osteoporosis is a severe medical condition characterized by low bone mass and deterioration of bone structure, which increase bone fragility and fracture risk [1]. Patients with osteoporosis can lose up to 50% of their bone density at critical skeletal locations [2]. His illness is now treated with RANK ligand antibodies (denosumab), selective estrogen receptor modulators (SERMs), teriparatide, and bisphosphonates [3]. Most of these drugs prevent bone remodeling by reducing osteoclast activity and recruiting new osteoclasts. Although these medications help treat and manage this condition, their long-term use has significant drawbacks. For example, long-term bisphosphonate therapy has been linked to atrial fibrillation, jaw osteonecrosis, and severe bone turnover inhibition [4]. Long-term SERM (raloxifene) use has also been linked to venous thromboembolism and fatal strokes [5]. Therefore, effective therapy is required to improve bone mineral density and generate new bone without significant side effects associated with long-term medication [6, 7]. Statins have anti-inflammatory properties, because they lower the levels of interleukin-6 and interleukin-8. Mundy demonstrated for the first time an experimental study in which statins improved bone volume. The trabecular bone volume increased in rats whose ovaries were removed and administered 5–10 mg simvastatin daily for 35 days [8].

Simvastatin, another statin medication, has been shown to increase the amount of bone tissue, the rate at which bone tissue is produced, and the strength of spongy bone tissue [9]. Several processes involved in statin drugs and bone metabolism are of particular interest. These substances stimulate osteoblast activity, which is stimulated by bone morphogenetic protein-2. Statins also inhibit hydroxymethylglutaryl coenzyme-A reductase and

lower mevalonate production, thereby interfering with osteoclast function and increasing apoptosis, which prevents bone resorption. Statins have an anti-inflammatory effect, causing bone defects in the affected bone and surrounding tissues. Statin use may also aid bone healing [10].

The effect of atorvastatin (ATV) on the proliferation, migration, and invasiveness of primary smooth muscle cells isolated from human saphenous veins after loading into a hyaluronic acid hydrogel was studied. The results show that the hydrogel is a viable substrate for local drug administration because it allows for the steady release of ATV over hours, resulting in multiple changes in the vascular smooth muscle cells phenotype that are similar to those produced by the drug freely dissolved in the cell environment [11]. Another study used a crosslinked hyaluronic acid hydrogel/poly(lactic-co-glycolic acid) microparticle formulation loaded with ATV to develop a simple drug delivery system to prevent intimal hyperplasia (IH). A carotid artery ligation model was used to validate the in vivo proof of concept. The combination of rapid and continuous ATV release has a synergistic effect on IH development. There was no evidence of harm to the collected tissues [10]. In another study, Özdoğan et al. [12] discovered that combining ATV with chitosan improved anti-inflammatory activity and bone and tissue healing in periodontitis-induced rats. Therefore, using osteoimmunomodulatory biomaterials to create a local immunological environment that promotes bone regeneration and osseointegration may be an appropriate method for redressing this imbalance [13]. Natural source-based materials are promising for biomedical applications [14–19]. Nanobiomaterials are made using biological resources such as fungi, plants, and algae [20–23]. Chitin, as a fibrous substance in the cell walls of some fungi, is the source of chitosan. The most important characteristics of chitosan are its nonantigenicity, excellent biodegradability, biocompatibility, ease of processing under mild conditions, interaction with cell matrix components and cell surface receptors, reactive and changeable groups, and chelating capacity. However, its controlled degradation ensured long-term survival of the encapsulated cells. In addition, chitosan can create a dynamic environment for penetration of tissue defects, making it a suitable option for use in delivery systems or matrices for the regeneration of different tissues [24]. In this study, we aim to design a sensitive, fast, and routine method that can be implemented at a low cost in the shortest time, and on the other hand, can be used as a platform that can be developed.

2. Materials and Methods

2.1. Materials. Sodium alginate (Catalog no. 501785611), chitosan (Catalog no. NC0805453), disodium phosphate, pentasodium tripolyphosphate (TPP; Catalog no. 106999), and sodium dihydrogen phosphate were purchased from Sigma–Aldrich. Dimethylformamide (Catalog no. 103034) and acetic acid (Catalog no. 137000) were acquired from Merck Co., whereas ATV calcium was acquired from Sobhandarou.

2.2. CS/ALG Hydrogel Fabrication. Chitosan (0.2 g) was dissolved in 10 ml acetic acid (1%) under stirring conditions for 15 min, and the alginate solution was then prepared by dissolving sodium alginate (0.45 g) in deionized water (10 ml, conductivity at 25°C = 0.02 μS/cm) under stirring conditions with magnetic stirrer (1,000 rpm) at room temperature for 15 min. The above solutions were mixed at a specific ratio and stirred overnight with a magnetic stirrer (1,200 rpm) at room temperature to obtain chitosan–alginate (CS/ALG) as the final product.

2.3. CS/ALG/TPP Hydrogel Fabrication. Chitosan (0.2 g) dissolved in 10 ml acetic acid (1%), sodium alginate (0.45 g) dissolved in distilled water, and TPP (0.01 g) as a crosslinker were mixed. The solutions were stirred overnight with a magnetic stirrer (1,200 rpm) at room temperature [25] (Figure 1).

2.4. Preparation of Drug-Loaded Hydrogel. To load the drug, chitosan (0.1 g) was dissolved in 10 ml of acetic acid (1%), sodium alginate (0.0225 g) in 10 ml of deionized water, TPP (0.005 g) in 2 ml of deionized water, ATV in 10 ml of deionized water, and dimethyl fumarate (3 ml) in 10 ml of deionized water. The solutions were then mixed and stirred using a magnetic stirrer (1,200 rpm) overnight at room temperature. Finally, the CS/ALG/TPP hydrogel containing ATV was obtained.

2.5. Release Study in Phosphate-Buffered Saline. Three samples (average weight = 19.66 g) of CS/ALG/TPP loaded with ART were dispersed in 25 ml of phosphate-buffered saline (PBS) (pH = 7.4). The hydrogels were then placed in a shaker incubator (80 rpm) at 37°C. At specific times, PBS (3 ml) containing ART in the buffer solution was removed, measured using a UV–visible at 241.5 nm, and resupplemented with a fresh 3 ml of PBS. A set of standard solutions was used to calibrate the amount of ART present at each time point. The actual drug concentration was determined using Equation (1) [26]:

$$Cn = Cn.\text{meas} + \frac{\Delta v}{Vt}\sum_{s=1}^{n-1}(Cs.\text{meas}), \quad (1)$$

where n, n^{th} concentration measurement; Cn, corrected drug concentration; Cn.meas, the acquired drug concentration at the n^{th} measurement; Δv, the withdrawn volume at each measurement; and Vt, the total volume of solution.

3. Physicochemical Properties of Hydrogels

3.1. Fourier Transform Infrared Spectroscopy. Fourier transform infrared spectroscopy (FTIR) (Equinox 55 LS 101, Bruker, Germany) was used to assess the chemical characteristics of the prepared CS/ALG/TPP. We used a wavelength range of 400–4,000 cm^{-1}, as in our previous work [27]. The Infrared (IR) spectra of all KBr-pressed samples were recorded in CO_2 nitrogen gas at room temperature [27].

3.2. Scanning Electron Microscopy of CS/ALG/TPP Hydrogel Loaded with ART. Scanning electron microscope (SEM) (LEO 1430 VP, Germany) was used to evaluate the surface morphology and structure of prepared material according to our previous works [28] at 15 kV acceleration voltage. Materials were sectioned into thin slices and vacuum-coated with Au–Pd thin layer by a Polaron SC7620 sputter coater as used previously [27].

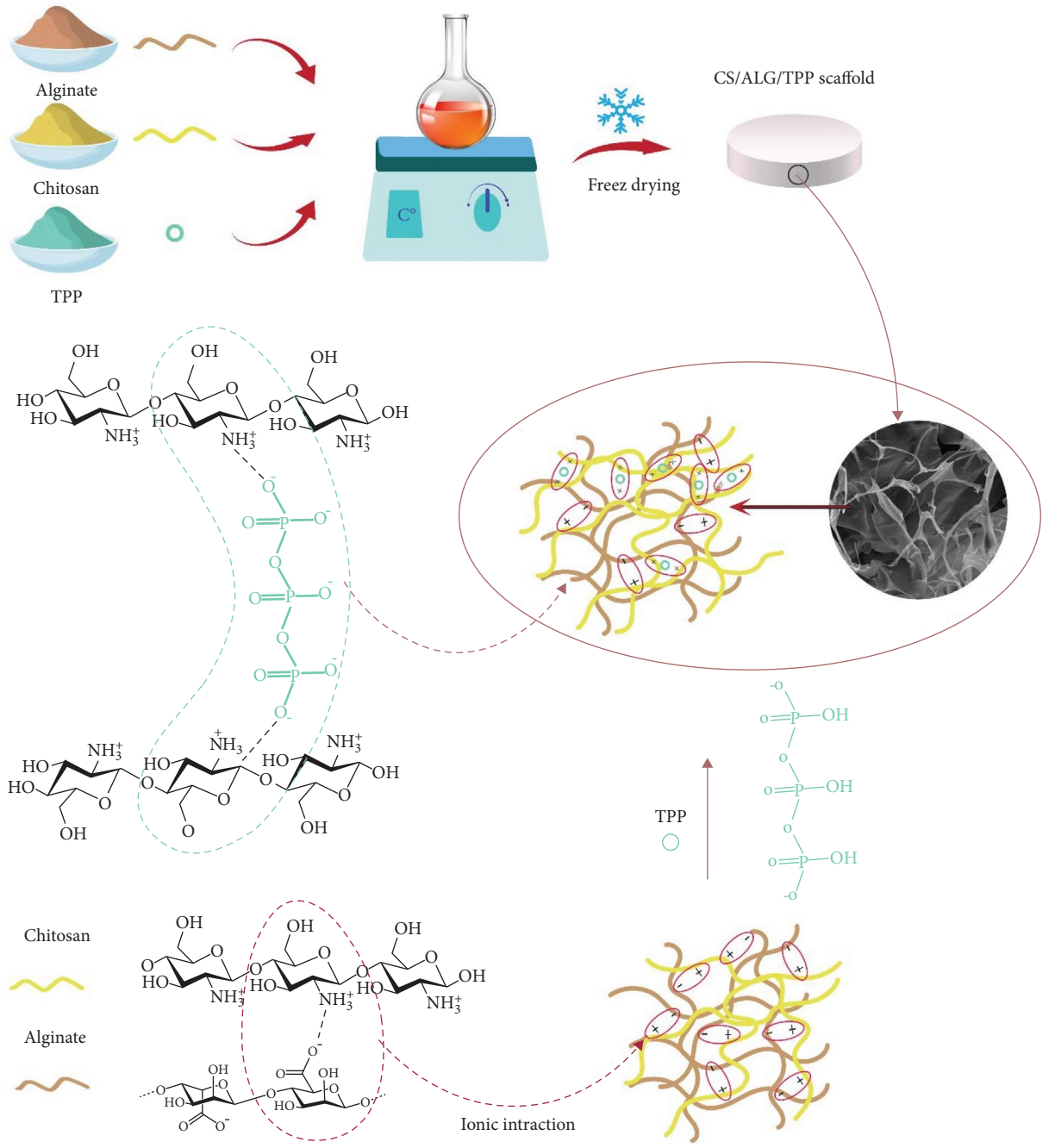

Figure 1: Schematic representation of the fabrication process of the CS/ALG/TPP scaffold.

3.3. Moisture Content and Swelling Ratio. To evaluate the swelling performance, freeze-dried hydrogel samples were immersed in PBS (pH 7.4) at 37°C and evaluated immediately after the liquid was removed from the hydrogel surface using a wet sponge. This process was repeated until total hydration was achieved. The swelling ratio (SR, g/g) was calculated using Equation (2) [25]:

$$\mathrm{SR}\,(\%) = \frac{W_s - W_d}{W_d} \times 100, \tag{2}$$

where W_d, hydrogel weight before floating in buffer (dry hydrogel) and W_s, weight of hydrogel after swelling in buffer (wet hydrogel).

4. Results and Discussion

4.1. Characterization of Fabricated CS/ALG/TPP Hydrogel. The hydrogels in this study were created by simply complexing chitosan, alginate, and TPP solutions (Figure 1). FTIR spectrometry was used to investigate the chemical structures of Gierszewska et al. [25]. One of the most important anionic

crosslinkers is TPP, which is widely used in the synthesis of scaffolds, membranes, nanoparticles, and various composites for medical purposes [29].

In addition, because phosphate groups are necessary for bone mineralization, TPP is widely used as a crosslinker in the development of biomimetic polymer systems for bone regeneration.

The degree of crosslinking can affect the homogeneity, porosity, hydrophilicity, and mechanical properties of scaffolds [30]. Consequently, a precise duration of the crosslinking stage is crucial for obtaining systems with exceptional performance. This negative phosphate crosslinker is frequently used to form positive ammonium chitosan crosslinks. Because instant gelation results in the formation of precipitates, simple mixing of chitosan and TPP solutions in tissue engineering applications is not an appropriate method for regulating the crosslinking reaction. Consequently, numerous methods for preparing CS-TPP systems with a controlled degree of crosslinking have been developed, such as those based on the ionic strength of the CS solvent in the presence of NaCl or the slow diffusion of TPP in the CS solution. This was used to create uniform membranes. In this study, CS/ALG scaffolds were crosslinked by immersion in TPP solution. To investigate the effects of various experimental conditions on scaffold performance, scaffolds were prepared with various concentrations of CS (1% and 2% w/w) and alginate, as well as two concentrations of TPP (1% and 2% w/w), and various reaction times (2, 4, and 8 hr). FTIR spectral range: the formation of chitosan crosslinks was confirmed by the crosslink scaffold composed of CS/ELG/TPP.

Figure 2(a)–2(c) depicts the FTIR spectra of chitosan, alginate, pentasodium TPP, and their mixtures [31].

Except for TPP, all spectra exhibited a strong and broad antisymmetric band at approximately 3,430 cm^{-1}, which was caused by the overlap of O–H and N–H stretching vibrations of the functional groups involved in hydrogen bonding. Chitosan possesses characteristic bands at 1,650 cm^{-1} (associated with the stretching vibrations of carbonyl amide 1), 1,598 cm^{-1} (associated with the bending vibrations of the first type of nonacetylated aminoglycoside), and 1,560 cm^{-1} (related to the bending vibrations of the N–H group of amide type 2).

Chitosan's saccharide structure is characterized by absorption bands at 2,253 cm^{-1} (asymmetric stretching vibrations of C–O–C bonds), 1,083 cm^{-1}, and 1,031 cm^{-1} (skeletal vibrations including C–O bonds). When chitosan was crosslinked with TPP, a new absorption band was observed at 1,635 cm^{-1}, owing to the antisymmetric vibration of N–H in the NH_2 groups. After the ion crosslinking of chitosan with TPP, additional changes in the IR spectrum were observed. The absorption at 1,215 cm^{-1} was due to the stretching vibrations of the C = O bond of the crossphosphate linker groups [25].

4.2. Swelling Study of CS/ALG/TPP Hydrogel. The SR was measured to evaluate the swelling performance of the prepared CS/ALG/TPP hydrogel containing ART and quantify its water uptake ability. The SR values of the prepared hydrogels are shown in Figure 3. Swelling is caused by liquid absorption by the polymer, and can be calculated by measuring the hydrogel mass. The mass SR data revealed that the Chit/Alg/TPP hydrogels exhibited 700%–800% swelling in the first few hours and 1,000% swelling after 30 hr, before decreasing to approximately 800% [32]. The swelling behavior and structural stability of hydrogels are critical for their practical use in tissue engineering. Most natural polymers, including chitosan, rapidly swell in biological fluids. Previous research indicates that early swelling is favorable and that the resulting increase in pore size promotes cell adhesion and development in a three-dimensional structure [33]. On the other hand, persistent swelling may result in loss of mechanical integrity and maceration of the surrounding tissue [32].

4.3. SEM Study of CS/ALG/TPP Hydrogel. SEM was used to investigate the morphological and surface properties of CS/ALG/TPP-containing ART hydrogels. Figure 4 shows the SEM images of the hydrogels. Images captured by SEM of the CS/ALG/TPP freeze-dried hydrogel containing ART revealed the morphology of the hydrogel. Examination of the hydrogel architecture revealed that the scaffold had a highly porous structure with interconnected pores generated by phase separation during lyophilization. The hydrogel structure is completely permeable. The holes are approximately 30 μm in size, which facilitates bone cell adhesion and development and is advantageous for cell attachment and migration [34].

4.4. Porosity Determination of CS/ALG/TPP Hydrogel. SEM was used to investigate the morphological and surface properties of CS/ALG/TPP-containing ART hydrogels. Figure 4 shows the SEM images of the hydrogels. Images captured by SEM of the CS/ALG/TPP freeze-dried hydrogel containing ART revealed the morphology of the hydrogel. Examination of the hydrogel architecture revealed that the scaffold had a highly porous structure with interconnected pores generated by phase separation during lyophilization. The hydrogel structure is completely permeable. The holes are approximately 30 μm in size, which facilitates bone cell adhesion and development and is advantageous for cell attachment and migration [35]:

$$P = \frac{(V_1 - V_3)}{(V_2 - V_3)} \times 100\%, \tag{3}$$

where $V_1 = 9$, $V_2 = 9.05$, $V_3 = 8.4$, and $P = 92\%$.

After crosslinking, the hydrogel was 92% porous (Figure 3), and after 24 hr in water, it swelled by a shock of 98.6%.

Numerous studies have reported the amount of water absorption and swelling of alginate and chitosan hydrogels crosslinked with TPP. After approximately 24 hr, the maximum swelling percentage of the crosslinked CS/ALG hydrogel was 98.6%, which is greater than the values reported in the literature [36, 37]. The results showed that using a TPP crosslinker is beneficial, and because the structure of the hydrogel is highly porous (92%), the expansion percentage can be significantly increased.

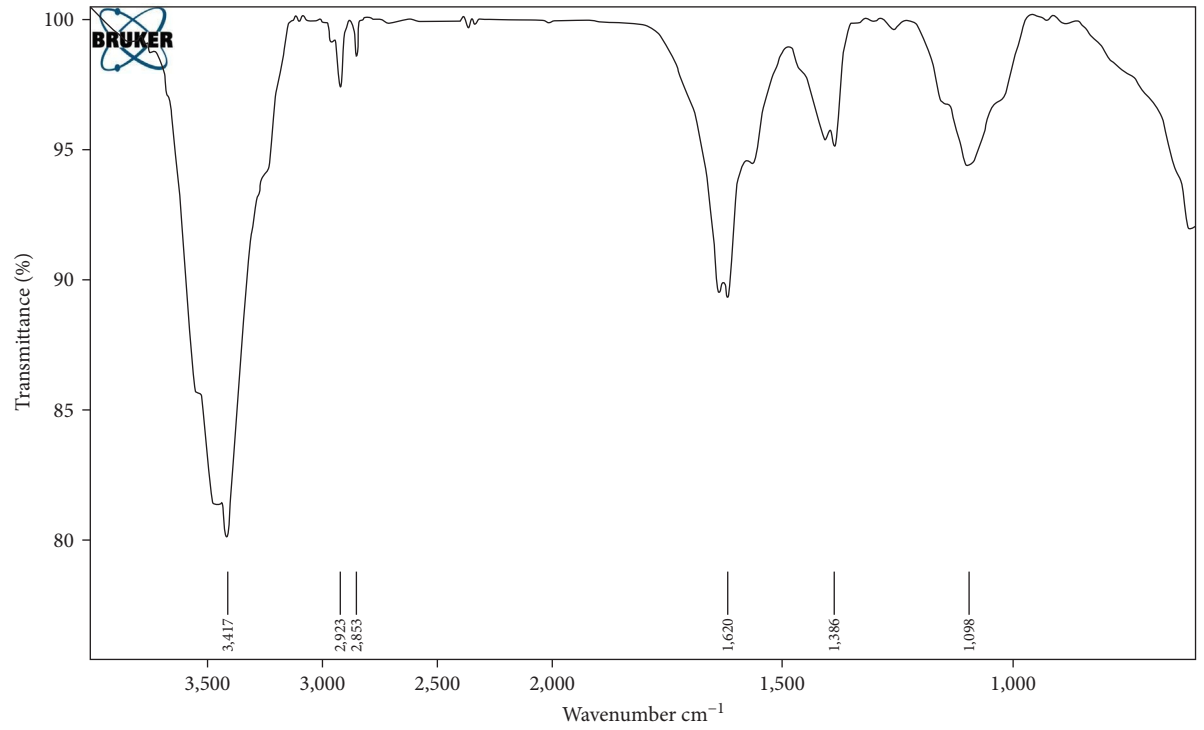

(a)

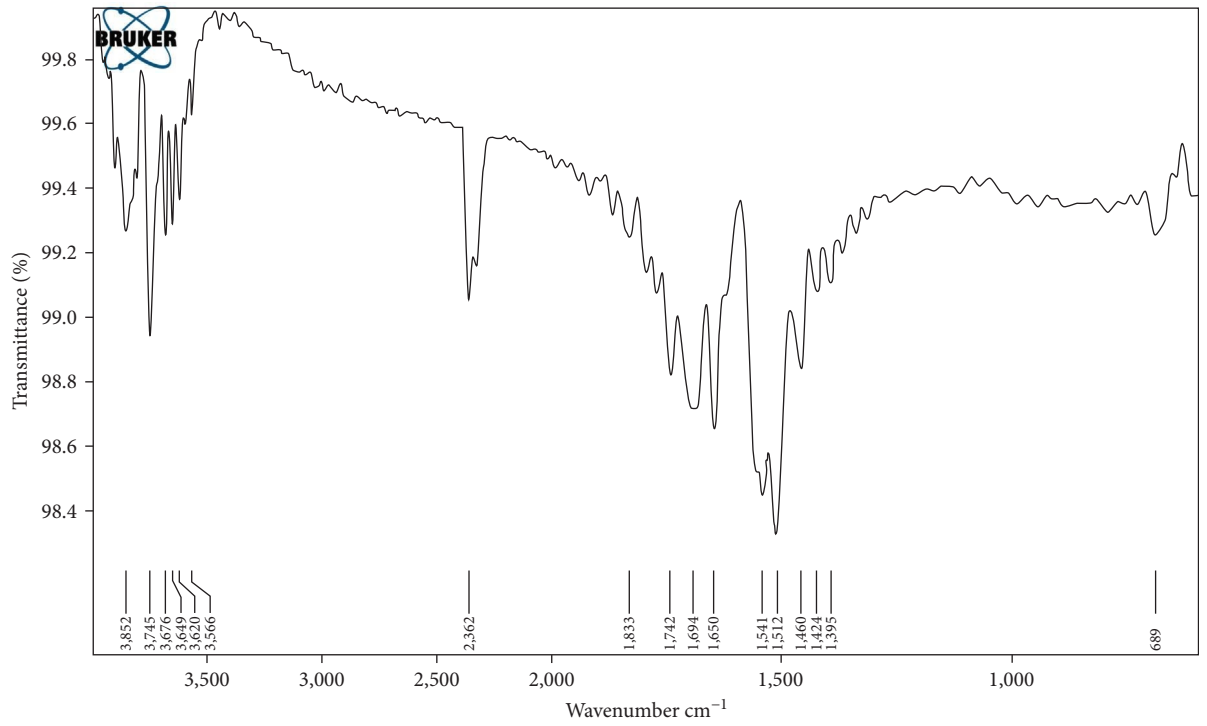

(b)

Figure 2: Continued.

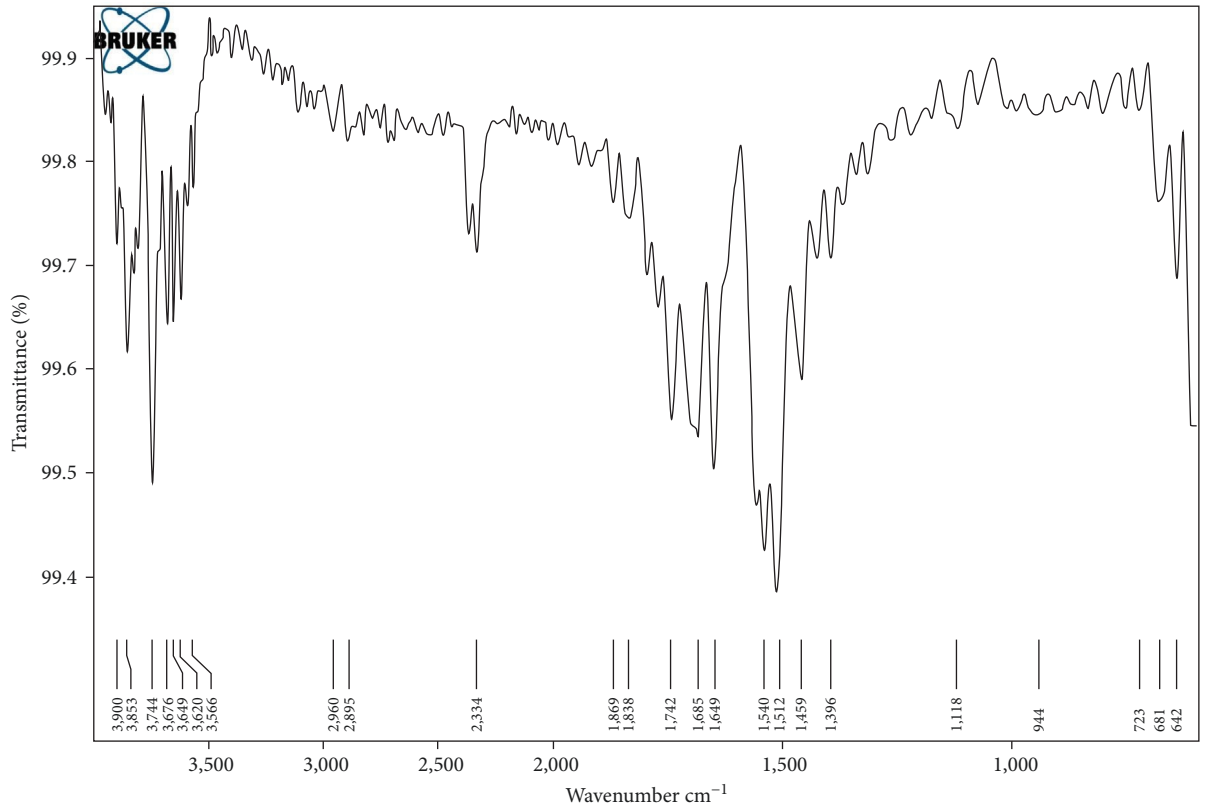

Figure 2: (a) FTIR spectrum of CS/ALG hydrogel, (b) FTIR spectra of CS/ALG/TPP hydrogel, and (c) FTIR spectra of CS/ALG/TPP scaffold containing ART.

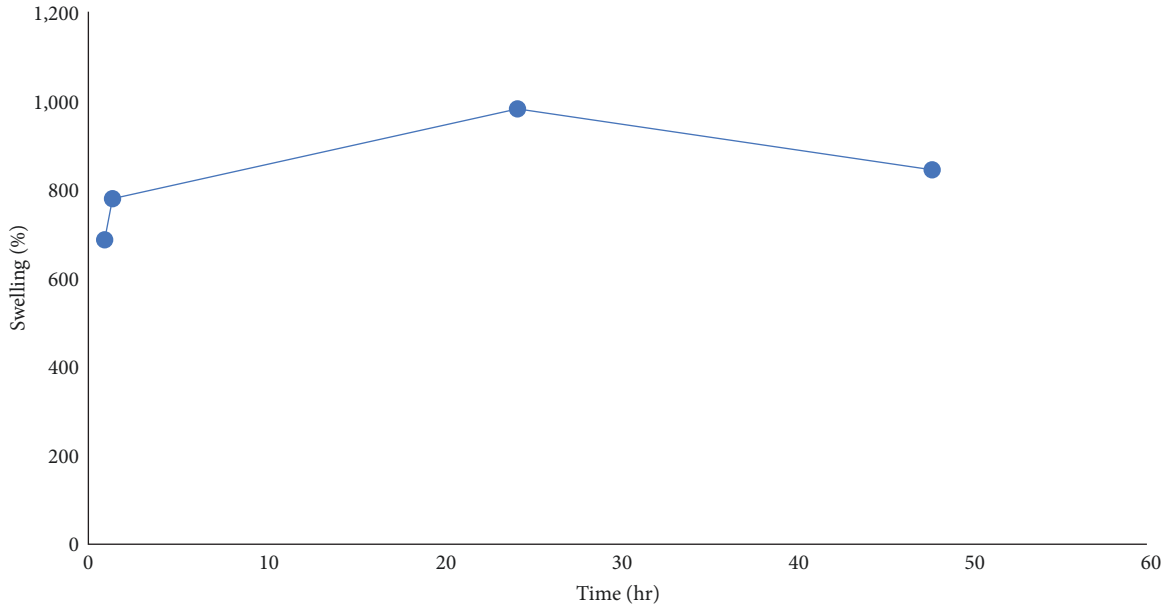

Figure 3: Swelling percentage graph of CS-AlG-TPP freeze-dried hydrogel containing atorvastatin in phosphate buffer after hours.

4.5. Cumulative Release Study. This study investigated the release of ART from CS/ALG/TPP hydrogels in PBS (pH 7.4) at 37°C for 10 and 24 hr (Figure 5). Standard deviations of the samples were calculated. The drug release profile was examined at 37°C and a pH of 7.4. The results revealed that the drug was released explosively in the first hour at approximately 25% (Figures 5(a) and 5(b)) and then gradually for 10 hr, at a rate of approximately 35%. After 24 hr,

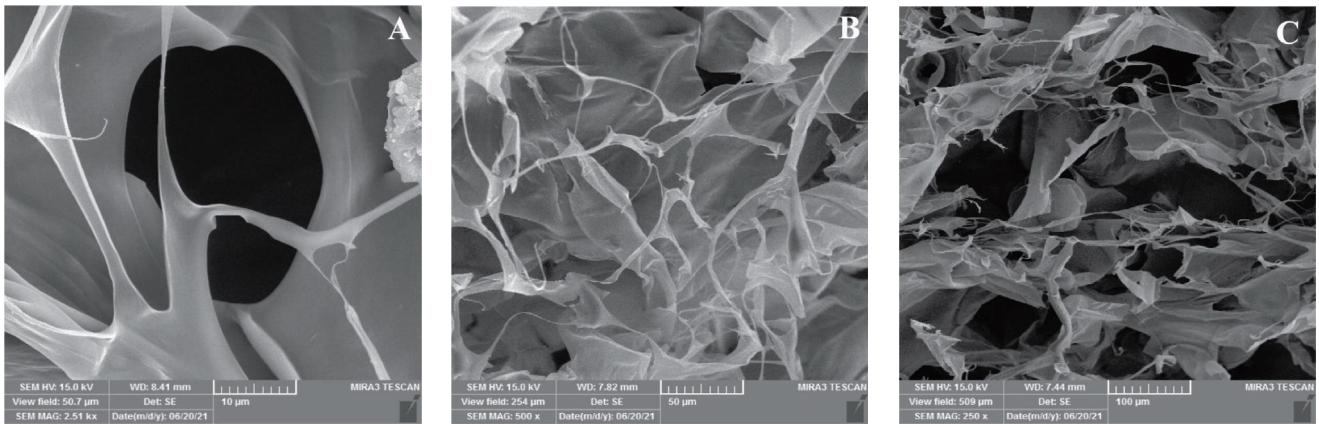

FIGURE 4: Scanning electron microscope images of CS-AlG-TPP freeze-dried hydrogel containing ATV with magnifications of (a) 10 μm, (b) 50 μm, and (c) 100 μm.

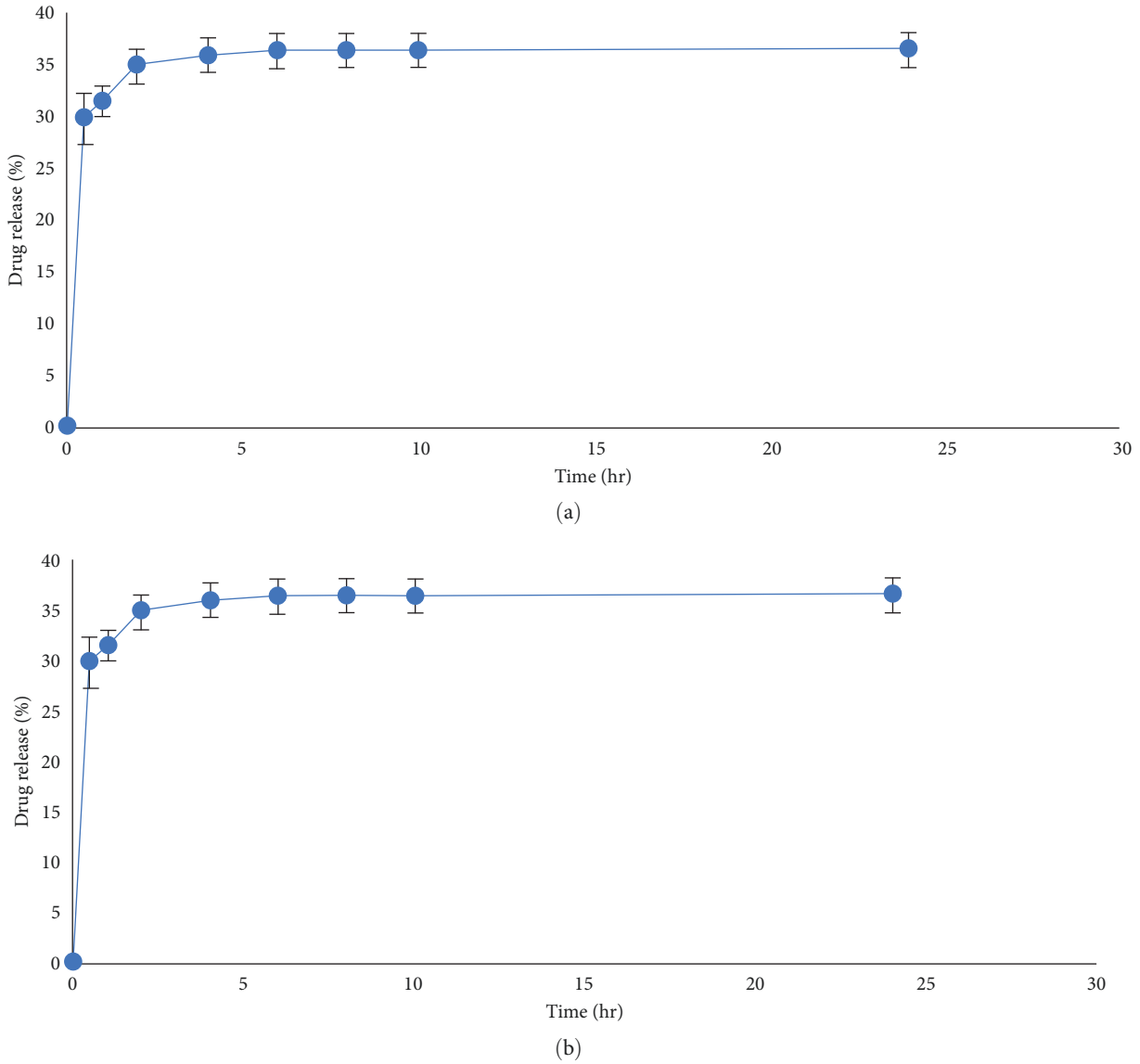

FIGURE 5: Graph of release percentage of atorvastatin in certain time intervals. (a) After 10 hr and (b) after 24 hr.

there was no significant increase in the percentage of drug released (Figure 5(b)). The gradual release of ATV from the alginate–chitosan microspheres was studied. Because TPP crosslinking does not occur in this system, the swelling percentage and amount of drug loading are lower, and drug release from these microspheres is slow and complete after 25 hr [38]. This suggests that the drug was retained in the three-dimensional network formed by TPP, and that the drug molecules entrapped within the porosity of the hydrogel were slowly released. During the first hour, 20% of the drug attached to the hydrogel is released via surface absorption. The percentage of crosslinkers significantly influenced the encapsulation gain and release profiles. Increasing the proportion of crosslinkers is expected to increase the proportion of drug loading while decreasing and limiting the proportion of drug release; thus, optimizing the proportion of crosslinkers is critical.

5. Conclusion

CS/ALG hydrogels were prepared and loaded with ATV at various ratios and percentages of TPP crosslinker. The results showed that the drug was loaded with an approximately 100% gain during crosslinking. The drug release profile from the hydrogel was investigated, and the results showed that the percentage of drug release was relatively low owing to drug retention in the three-dimensional TPP network. The results of this study demonstrated that the crosslinked CS/ALG hydrogel could be a suitable scaffold for loading all types of drugs, macromolecules, and cells because of its swelling percentage and high porosity. The drug loading and percentage of release are expected to be controlled by adjusting the ratio of the two polymers and crosslinker. Future studies should consider scaffold cell compatibility tests, such as hemolysis and cytotoxicity. Furthermore, stability studies, biodegradability determination, and modification of the drug release profile via a change in the crosslinker ratio will help to improve this study. Finally, the scaffolds mentioned above can be studied further in cell and animal studies for bone tissue engineering and stem cell differentiation in the presence of ATV.

Data Availability

The data used to support the findings of this study have been included in this article.

Conflicts of Interest

The authors declare that they have no conflicts of interest.

Authors' Contributions

Hananeh Hamedfar and Tayebeh Zivari Ghader contributed equally to this work.

Acknowledgments

The authors are grateful for the financial support of the Tabriz University of Medical Sciences, Tabriz, Iran. Grant no. 4221 was provided by the Department of Medicinal Chemistry, Faculty of Pharmacy, Tabriz University of Medical Sciences, Tabriz, Iran.

References

[1] S. L. Bonnick, "Osteoporosis in men and women," *Clinical Cornerstone*, vol. 8, no. 1, pp. 28–39, 2006.

[2] M. Shahrezaee, A. Oryan, F. Bastami, S. Hosseinpour, M. H. Shahrezaee, and A. Kamali, "Comparative impact of systemic delivery of atorvastatin, simvastatin, and lovastatin on bone mineral density of the ovariectomized rats," *Endocrine*, vol. 60, no. 1, pp. 138–150, 2018.

[3] G. Mazziotti, J. Bilezikian, E. Canalis, D. Cocchi, and A. Giustina, "New understanding and treatments for osteoporosis," *Endocrine*, vol. 41, no. 1, pp. 58–69, 2012.

[4] K. A. Kennel and M. T. Drake, "Adverse effects of bisphosphonates: implications for osteoporosis management," *Mayo Clinic Proceedings*, vol. 84, no. 7, pp. 632–638, 2009.

[5] W. Ledger and P. C. Ho, *Gynecological Drug Therapy*, p. 315, CRC Press, Boca Raton, 1st edition, 2016.

[6] A. Oryan, A. Kamali, and A. Moshiri, "Potential mechanisms and applications of statins on osteogenesis: current modalities, conflicts and future directions," *Journal of Controlled Release*, vol. 215, pp. 12–24, 2015.

[7] A. Moshiri, M. Shahrezaee, B. Shekarchi, A. Oryan, and K. Azma, "Three-dimensional porous gelapin–simvastatin scaffolds promoted bone defect healing in rabbits," *Calcified Tissue International*, vol. 96, no. 6, pp. 552–564, 2015.

[8] G. Mundy, R. Garrett, S. Harris et al., "Stimulation of bone formation in vitro and in rodents by statins," *Science*, vol. 286, no. 5446, pp. 1946–1949, 1999.

[9] M. Takenaka, K. Hirade, K. Tanabe et al., "Simvastatin stimulates VEGF release via p44/p42 MAP kinase in vascular smooth muscle cells," *Biochemical and Biophysical Research Communications*, vol. 301, no. 1, pp. 198–203, 2003.

[10] I. Mylonaki, F. Strano, S. Deglise et al., "Perivascular sustained release of atorvastatin from a hydrogel-microparticle delivery system decreases intimal hyperplasia," *Journal of Controlled Release*, vol. 232, pp. 93–102, 2016.

[11] C. Dubuis, L. May, F. Alonso et al., "Atorvastatin-loaded hydrogel affects the smooth muscle cells of human veins," *Journal of Pharmacology and Experimental Therapeutics*, vol. 347, no. 3, pp. 574–581, 2013.

[12] A. I. Özdoğan, Y. D. İlarslan, K. Kösemehmetoğlu et al., "In vivo evaluation of chitosan based local delivery systems for atorvastatin in treatment of periodontitis," *International Journal of Pharmaceutics*, vol. 550, no. 1-2, pp. 470–476, 2018.

[13] X. Yin, C. Yang, Z. Wang et al., "Alginate/chitosan modified immunomodulatory titanium implants for promoting osteogenesis in vitro and in vivo," *Materials Science and Engineering: C*, vol. 124, Article ID 112087, 2021.

[14] P. Vahedi, R. Moghaddamshahabi, T. J. Webster et al., "The use of infrapatellar fat pad-derived mesenchymal stem cells in articular cartilage regeneration: a review," *International Journal of Molecular Sciences*, vol. 22, no. 17, Article ID 9215, 2021.

[15] A. Nasibova, "Generation of nanoparticles in biological systems and their application prospects," *Advances in Biology & Earth Sciences*, vol. 8, no. 2, pp. 140–146, 2023.

[16] V. Ramazanli, "Effect of pH and temperature on the synthesis of silver nano particles extracted from olive leaf," *Advances in Biology & Earth Sciences*, vol. 6, no. 2, 2021.

[17] I. Ahmadov and V. Ramazanli, "Synthesis of nanoparticles in biological systems and their physical chemical characteristics-green synthesis," *Advances in Biology & Earth Sciences*, vol. 4, no. 3, 2019.

[18] A. Jafarova and V. Ramazanli, "Antibacterial characteristics of Ag nanoparticle extracted from olive leaf," *Advances in Biology & Earth Sciences*, vol. 5, no. 3, 2020.

[19] E. Ahmadian, A. Eftekhari, D. Janas, and P. Vahedi, "Nanofiber scaffolds based on extracellular matrix for articular cartilage engineering: a perspective," *Nanotheranostics*, vol. 7, no. 1, pp. 61–69, 2023.

[20] A. Baran, M. Fırat Baran, C. Keskin et al., "Investigation of antimicrobial and cytotoxic properties and specification of silver nanoparticles (AgNPs) derived from *Cicer arietinum* L. green leaf extract," *Frontiers in Bioengineering and Biotechnology*, vol. 10, Article ID 855136, 2022.

[21] A. Baran, M. F. Baran, C. Keskin et al., "Ecofriendly/rapid synthesis of silver nanoparticles using extract of waste parts of artichoke (*Cynara scolymus* L.) and evaluation of their cytotoxic and antibacterial activities," *Journal of Nanomaterials*, vol. 2021, Article ID 2270472, 10 pages, 2021.

[22] M. F. Baran, C. Keskin, A. Baran et al., "Green synthesis of silver nanoparticles from *Allium cepa* L. peel extract, their antioxidant, antipathogenic, and anticholinesterase activity," *Molecules*, vol. 28, no. 5, Article ID 2310, 2023.

[23] A. Baran, C. Keskin, M. F. Baran et al., "Ecofriendly synthesis of silver nanoparticles using ananas comosus fruit peels: anticancer and antimicrobial activities," *Bioinorganic Chemistry and Applications*, vol. 2021, Article ID 2058149, 8 pages, 2021.

[24] T. Zivari-Ghader, S. Dolati, A. Mehdizadeh, S. Davaran, M. R. Rashidi, and M. Yousefi, "Recent scaffold-based tissue engineering approaches in premature ovarian failure treatment," *Journal of Tissue Engineering and Regenerative Medicine*, vol. 16, no. 7, pp. 605–620, 2022.

[25] M. Gierszewska, J. Ostrowska-Czubenko, and E. Chrzanowska, "Characteristics of ascorbic acid release from TPP-crosslinked chitosan/alginate polyelectrolyte complex membranes," *Progress on Chemistry and Application of Chitin and its Derivatives*, vol. 23, pp. 76–87, 2018.

[26] F. Esmaeili and M. Babazadeh, "Targeted and controlled release of indomethacin from polyacrylic carrier systems," *Der Pharmacia Lettre*, vol. 7, no. 2, pp. 40–48.

[27] F. Rad, S. Davaran, M. Babazadeh, A. Akbarzadeh, and H. Pazoki-Toroudi, "Biodegradable electrospun polyester-urethane nanofiber scaffold: codelivery investigation of doxorubicin-ezetimibe and its synergistic effect on prostate cancer cell line," *Journal of Nanomaterials*, vol. 2022, Article ID 8818139, 10 pages, 2022.

[28] S. Same, J. Kadkhoda, G. Navidi et al., "The fabrication of halloysite nanotube-based multicomponent hydrogel scaffolds for bone healing," *Journal of Applied Biomaterials & Functional Materials*, vol. 20, Article ID 22808000221111875, 2022.

[29] I. Silvestro, I. Francolini, V. Di Lisio et al., "Preparation and characterization of TPP-chitosan crosslinked scaffolds for tissue engineering," *Materials*, vol. 13, no. 16, Article ID 3577, 2020.

[30] S. Shahi, F. Dehghani, E. D. Abdolahinia et al., "Effect of gelatinous spongy scaffold containing nano-hydroxyapatite on the induction of odontogenic activity of dental pulp stem cells," *Journal of King Saud University—Science*, vol. 34, no. 8, Article ID 102340, 2022.

[31] M. Gierszewska-Drużyńska and J. Ostrowska-Czubenko, "The effect of ionic crosslinking on thermal properties of hydrogel chitosan membranes," *Progress on Chemistry and Application of Chitin and its Derivatives*, vol. 15, pp. 25–32, 2010.

[32] A. Ehterami, M. Salehi, S. Farzamfar et al., "Chitosan/alginate hydrogels containing alpha-tocopherol for wound healing in rat model," *Journal of Drug Delivery Science and Technology*, vol. 51, pp. 204–213, 2019.

[33] N. Shanmugasundaram, P. Ravichandran, P. N. Reddy, N. Ramamurty, S. Pal, and K. P. Rao, "Collagen–chitosan polymeric scaffolds for the in vitro culture of human epidermoid carcinoma cells," *Biomaterials*, vol. 22, no. 14, pp. 1943–1951, 2001.

[34] S. Yang, K. F. Leong, Z. Du, and C. K. Chua, "The design of scaffolds for use in tissue engineering. Part I. Traditional factors," *Tissue Engineering*, vol. 7, no. 6, pp. 679–689, 2001.

[35] Z. Wang, T. Gao, L. Cui, Y. Wang, P. Zhang, and X. Chen, "Improved cellular infiltration into 3D interconnected microchannel scaffolds formed by using melt-spun sacrificial microfibers," *RSC Advances*, vol. 6, no. 3, pp. 2131–2134, 2016.

[36] H. Hamedi, S. Moradi, A. E. Tonelli, and S. M. Hudson, "Preparation and characterization of chitosan–alginate polyelectrolyte complexes loaded with antibacterial thyme oil nanoemulsions," *Applied Sciences*, vol. 9, no. 18, Article ID 3933, 2019.

[37] M. Tavakol, E. Vasheghani-Farahani, and S. Hashemi-Najafabadi, "The effect of polymer and $CaCl_2$ concentrations on the sulfasalazine release from alginate-*N*,*O*-carboxymethyl chitosan beads," *Progress in Biomaterials*, vol. 2, no. 1, pp. 1–8, 2013.

[38] A. M. Gorabi, N. Kiaie, M. Pirro, V. Bianconi, T. Jamialahmadi, and A. Sahebkar, "Effects of statins on the biological features of mesenchymal stem cells and therapeutic implications," *Heart Failure Reviews*, vol. 26, no. 5, pp. 1259–1272, 2021.